ChemPubSoc Europe

DOI: 10.1002/chem.201704303

CHEMISTRY A European Journal Full Paper

Batteries

A Promising High-Voltage Cathode Material Based on Mesoporous $Na_3V_2(PO_4)_3$/C for Rechargeable Magnesium Batteries

Jing Zeng, Yang Yang, Shaobo Lai, Jianxing Huang, Yiyong Zhang, Jing Wang, and Jinbao Zhao*[a]

Abstract: The lack of suitable high-voltage cathode materials has hindered the development of rechargeable magnesium batteries (RMBs). Here, mesoporous $Na_3V_2(PO_4)_3$/C (NVP/C) spheres have been synthesized through a facile spray-drying–annealing method, and their electrochemically desodiated phase $NaV_2(PO_4)_3$/C (ED-NVP/C) has been investigated as an intercalation host for Mg^{2+} ions. The obtained ED-NVP/C exhibits an average discharge voltage of around 2.5 V (vs. Mg^{2+}/Mg), higher than those of most previously reported cathode materials. In addition, it can deliver an initial discharge capacity of 88.8 mA h g^{-1} at 20 mA g^{-1}, with good cycling stability. Ex situ X-ray diffraction (XRD) and X-ray photoelectron spectroscopy (XPS) results demonstrate that the electrochemical reaction is based on an intercalation mechanism and shows good reversibility. Galvanostatic intermittent titration technique (GITT) data have revealed that the intercalation process involves a two-phase transition. The reported ED-NVP/C cathode material with high working voltage offers promising potential for application in RMBs.

Introduction

Li-ion batteries (LIBs) can be considered as a successful achievement in the field of electrochemical power sources, and they are widely used in mobile devices. However, their high cost, relatively low energy density, and safety problems limit their application in large-scale mobile and stationary devices.[1] Recently, rechargeable magnesium batteries (RMBs) have attracted increased attention as a potential alternative to LIBs. Compared to Li-containing anodes, the deposition of Mg on an anode is dendrite-free and Mg is safer when exposed to air. Thus, Mg can be directly used as an anode with good safety.[2] Additionally, Mg provides a high volumetric energy density of 3832 mA h cm^{-3} (cf. 2062 mA h cm^{-3} for Li) due to the two-electron reaction mechanism. Moreover, Mg is more abundant and cheaper than Li, which is beneficial for reducing the cost of battery production.[3] However, the slow electrode kinetics resulting from the sluggish diffusion of Mg^{2+} ions in solid materials has impeded development, and the identification of suitable cathode materials is still highly desired. The Chevrel phase Mo_6S_8 has been regarded as a promising cathode material for RMBs, offering excellent cycle performance.[4] However, the low working voltage (ca. 1.1 V vs. Mg^{2+}/Mg) results in relatively low energy density, making it an unsatisfactory cathode material for commercial application. Improving the operating voltage is effective in improving the energy density since this parameter is obtained by multiplying the specific capacity by the average cell voltage. Unfortunately, most of the hitherto studied cathode materials have delivered a relatively low working voltage (< 2 V vs. Mg^{2+}/Mg), such as V_2O_5 (ca. 1.35 V),[5] MnO_2 (ca. 1.5 V),[6] $MgCoSiO_4$ (ca. 1.6 V),[7] and MoS_2 (ca. 1.0 V).[8] Although a few high-voltage cathode materials have been developed, the electrochemical performances of these materials have been less than satisfactory. High working temperature and low discharge–charge current density are usually needed to obtain relatively good electrochemical performance.[9] For instance, spinel oxide $MgCo_2O_4$ delivered a high operating voltage of around 2.9 V (vs. Mg^{2+}/Mg) and a discharge capacity of 200 mA h g^{-1}, but the operating temperature was as high as 150 °C and the current density was very low (0.02 C).[9a] $V_2(PO_4)_3$, prepared by electrochemical delithiation of monoclinic $Li_3V_2(PO_4)_3$ as an Mg^{2+} ion insertion host, exhibited an average working voltage of around 2.9 V (vs. Mg^{2+}/Mg) at 55 °C, again with a low current density.[9b] Thus, there is an urgent need for the development of new high-voltage cathode materials with good electrochemical performance for use in RMBs.

Rhombohedral $Na_3V_2(PO_4)_3$ (denoted as NVP), with an Na-superionic conductor (NASICON) structure, is a promising cathode material for sodium-ion batteries (SIBs) with a high discharge voltage plateau of around 3.34 V (vs. Na^+/Na).[10] It is built on the three-dimensional (3D) framework of PO_4 tetrahedra sharing corners with VO_6 octahedra, and forms a lantern-like structure in which Na^+ ions occupy the 6b sites (M1, C.N. = 6, Na1; C.N. = coordinate number) and 18e sites (M2,

[a] J. Zeng, Y. Yang, S. Lai, J. Huang, Y. Zhang, J. Wang, Prof. J. Zhao
State Key Laboratory of Physical Chemistry of Solid Surfaces
Collaborative Innovation Center of Chemistry for Energy Materials
State-Province Joint Engineering Laboratory of Power Source Technology for New Energy Vehicle
College of Chemistry and Chemical Engineering
Xiamen University, Xiamen, Fujian (P. R. China)
E-mail: jbzhao@xmu.edu.cn

Supporting information and the ORCID identification number for the author of this article can be found under https://doi.org/10.1002/chem.201704303.

C.N. = 6, Na2) (Scheme 1). The large open 3D framework of the NASICON structure, with a large interstitial space, allows rapid ion diffusion. When two Na2 cations are extracted from the NVP, a new phase, desodiated $NaV_2(PO_4)_3$ (ED-NVP), is formed,

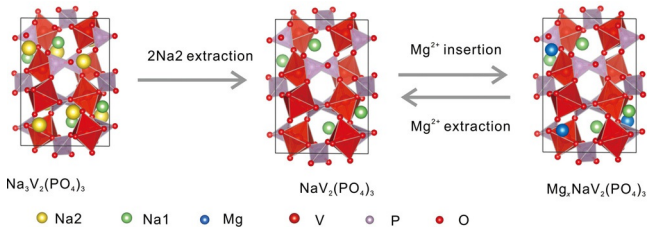

Scheme 1. Illustration of the electrochemical desodiation and (de)magnesiation processes.

providing a theoretical capacity of 118 mA h g^{-1} in SIBs. It is noteworthy that the skeleton structure of NVP remains intact during the Na^+ extraction process, contributing to its excellent electrochemical performance.[11]

Although NVP has been well studied as a cathode material for monovalent metal ions (Na^+, Li^+), its electrochemical performance with polyvalent ions has rarely been investigated.[12] Huang's group developed a zinc-ion battery based on an NVP cathode in aqueous electrolyte, indicating the feasibility of NVP serving as an intercalation host for polyvalent ions, including Zn^{2+}, Ni^{2+}, and Mg^{2+}.[13] Yao's group reported that ED-NVP in magnesium aluminum chloride complex (MACC) solution (0.2 M $[Mg_2(\mu\text{-}Cl)_2][AlCl_4]_2$/DME; DME = 1,2-dimethoxyethane), in which the active Mg cations are $MgCl^+$ and $Mg_2Cl_3^+$, however, showed poor electrochemical performance.[14] Since the strong, ionic Mg–Cl bonds of $MgCl^+$ and $Mg_2Cl_3^+$ have to be broken to give free Mg^{2+} ions for the subsequent intercalation process, additional barriers usually need to be overcome for Mg^{2+} ions to intercalate into transition metal oxides in such electrolytes.[15] Thus, a conventional electrolyte (a simple Mg salt, such as $Mg(ClO_4)_2$ or $Mg(TFSI)_2$ (TFSI = $C_2F_6NO_4S_2$) in a polar aprotic solvent) containing more weakly coordinating anions is probably more suitable to test the electrochemical performance of NVP. Recently, Tirado's group reported the electrochemical behavior of NVP in $Mg(TFSI)_2$/DME and proved that the insertion of Mg^{2+} ions into the ED-NVP structure is possible in a nonaqueous electrolyte. However, the insertion voltage of Mg^{2+} ions was low (ca. 1.2 V vs. Mg^{2+}/Mg) and the cycle performance was poor, with only 60 mA h g^{-1} remaining after 100 cycles in an Na–Mg hybrid electrolyte.[16] Due to the poor electronic conductivity of NVP, improving its conductivity by carbon coating is an effective way to improve its electrochemical performance.[17] Although much effort has been devoted to synthesizing NVP/C composites with good electrochemical performance, the preparation processes are rather complicated. For example, Mai's group reported a 3D NVP nanofiber network (NVP-F) prepared by a self-sacrificing synthesis.[18] Yu's group prepared carbon-coated nanosized NVP by a polyol process followed by heat treatment.[19] Thus, a facile and efficient synthetic method for preparing NVP/C is necessary. Spray-drying is a rapid, convenient, and reproducible method for synthesizing spherical particles that are agglomerate-free, and has been widely used in the preparation of electrode materials.[20] Indeed, our group has prepared several Li_3VO_4/C composites for Li^+ or Mg^{2+} ion storage by a spray-drying–annealing method, which showed good electrochemical performances.[21]

In this work, mesoporous NVP/C spheres have been synthesized by a facile spray-drying–annealing method. Two Na^+ ions were electrochemically removed from the unit cell of NVP/C, and the resultant phase ED-NVP/C was investigated as a cathode material for RMBs (Scheme 1). ED-NVP/C showed good electrochemical performance in RMBs with $Mg(TFSI)_2$/MeCN as the electrolyte. It delivered an average working voltage of around 2.5 V (vs. Mg^{2+}/Mg), much higher than that previously reported (1.2 V vs. Mg^{2+}/Mg). The discharge capacity was 88.8 mA h g^{-1} in the first cycle, and was maintained at 77 mA h g^{-1} after 100 cycles.

Results and Discussion

Preparation and characterization of NVP/C

The preparation process of NVP/C is shown in Scheme 2. Droplets composed of NH_4VO_3, $NH_4H_2PO_4$, CH_3COONa, and sucrose were expelled from the spray nozzle. The water in these droplets evaporated quickly, and the remaining solute condensed to form microspheres. After heat treatment, the final product

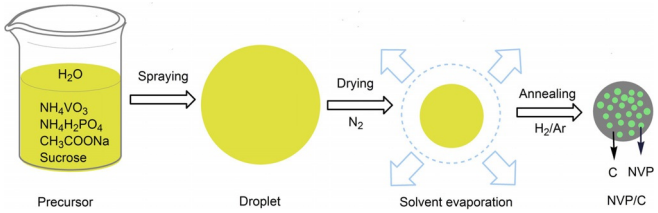

Scheme 2. The preparation process of the NVP/C.

NVP/C was obtained. Figure 1a shows the XRD pattern of the NVP/C. All of the diffraction peaks could be indexed to rhombohedral crystalline $Na_3V_2(PO_4)_3$ with space group *R*-3*c* (JCPDS No. 053-0018), and no impurities were observed. Sucrose served as a carbon source, which improved the electronic conductivity of the composite and inhibited the growth of NVP crystals (Figure S1 in the Supporting Information). Raman spectroscopy was used to verify the presence of carbon in the NVP/C (Figure 1b). For the pristine NVP, the bands at wavenumbers below 1100 cm^{-1} correspond to the Raman fingerprint of $Na_3V_2(PO_4)_3$. Two strong peaks at 1049 and 451 cm^{-1} can be attributed to a stretching vibration and a symmetrical bending mode, respectively, of PO_4 tetrahedra. The bands below 400 cm^{-1} correspond to the external modes of PO_4 and/or VO_6 polyhedra.[17b,22] For NVP/C, the D-band at 1355 cm^{-1} and the G-band at 1602 cm^{-1} are typical Raman features of carbon materials. The intensity ratio of G-band to D-band ($R = I_G/I_D$) is 1.15, suggesting that sucrose was partially graphitized

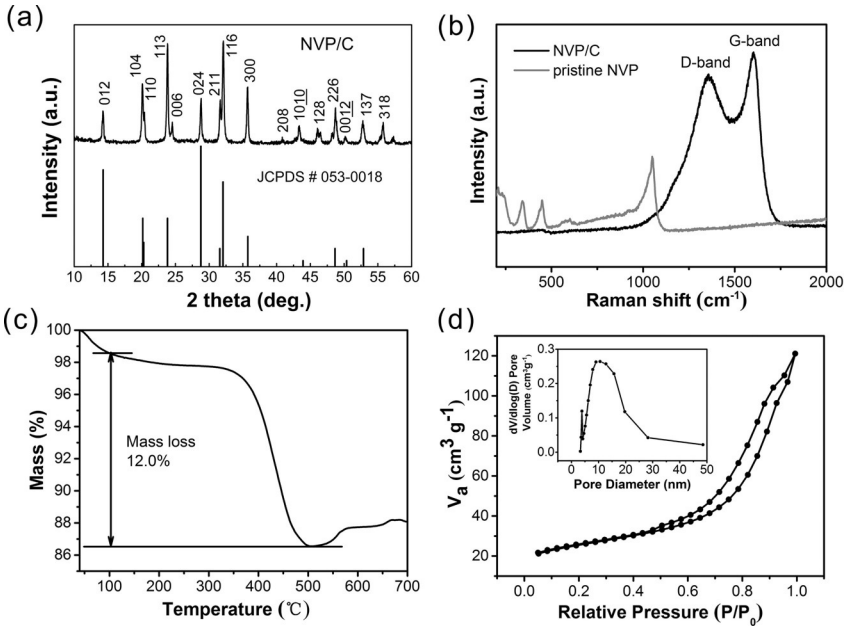

Figure 1. (a) XRD pattern of the NVP/C; (b) Raman spectra of NVP/C and pristine NVP; (c) TG curve of NVP/C in air atmosphere; (d) N_2 adsorption–desorption isotherms and corresponding pore size distribution (inset) of the NVP/C.

during the heat treatment.[23] The disappearance of the $Na_3V_2(PO_4)_3$ Raman fingerprint due to the screening effect of carbon suggests that $Na_3V_2(PO_4)_3$ particles in the NVP/C were well coated by a carbon layer.[22] The TG curve (Figure 1c) indicated that the carbon content of the NVP/C was around 12.0%. Nitrogen adsorption and desorption isotherms of the NVP/C (Figure 1d) yielded a type IV curve. The specific surface area was evaluated as 85.34 $m^2 g^{-1}$. The pore size distribution (Figure 1d, inset) revealed that the NVP/C had a mesoporous structure with two distinct pore diameter distributions: larger pores in the range 8–35 nm and smaller pores of about 4 nm. The high specific surface area and mesoporous structure favor penetration of the electrolyte and can shorten the diffusion paths for Mg^{2+} ions during the electrochemical process.

The morphology and microstructure of the NVP/C were investigated by SEM and TEM. An SEM image (Figure 2a) shows that the obtained NVP/C sample consisted of spheres with diameters in the range 0.5–4 μm. A TEM image (Figure 2b) further confirmed the spherical structure. An HRTEM image (Figure 2c) showed that the NVP particles were coated with a thin layer of carbon of about 10 nm. The obvious lattice fringes of carbon on the surface of the NVP/C particles revealed that part of the carbon was graphitized (denoted as g-C), consistent with the Raman results. The interplanar distance of the NVP particles was measured as 0.25 nm, corresponding to the *d*-spacing of the (300) planes of the rhombohedral $Na_3V_2(PO_4)_3$. Elemental mapping results (Figure 2d) indicated that all of the elements were uniformly distributed within the NVP/C particles. The above analyses fully supported the successful synthesis of mesoporous NVP/C spheres.

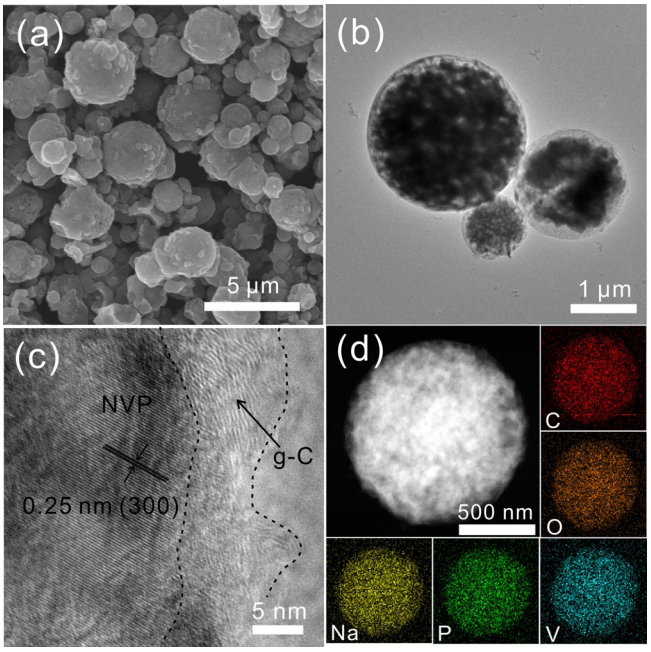

Figure 2. (a) SEM image of the NVP/C; (b) TEM; and (c) HRTEM images of the NVP/C (g-C represents graphitized carbon); (d) high-angle annular dark-field (HAADF)-TEM image, and elemental mappings of C, O, Na, P, and V, respectively.

Electrochemical performance

It has been reported that the expected voltage in Mg batteries is about 1 V lower than that in Li batteries with the same host.[24] Since the discharge voltage of NVP is about 3.6 V (vs. Li^+/Li) in Li batteries, the expected voltage in Mg batteries would be about 2.6 V (vs. Mg^{2+}/Mg).[24,25] However, a discharge

voltage of only 1.2 V (vs. Mg^{2+}/Mg) has been reported when using Mg metal as both the counter and reference electrodes in $Mg(TFSI)_2$/DME.[16] A similar result was also obtained in our work when using 0.5 M $Mg(ClO_4)_2$/MeCN as the electrolyte and Mg metal as the anode in a two-electrode coin cell (Figure S2). The electrolyte may have been the cause of this situation, since a thick passive layer will form on an Mg anode in these conventional electrolytes.[16] Thus, a more appropriate electrochemical test system was needed to evaluate the electrochemical performance of ED-NVP/C. The $Mg(TFSI)_2$/MeCN system is commonly chosen as the electrolyte to examine the electrochemical performances of high-voltage cathode materials. Due to its incompatibility with an Mg anode, AC electrodes with large specific area are chosen as both the counter and reference electrodes. Fast and fully reversible ion adsorption/desorption can take place on an AC counter electrode; that is, anions ($TFSI^-$) adsorb on the AC electrode during the discharge process and desorb during the charge process.[5] Since the potential of an AC electrode is rather stable in an MeCN-based system, it can also serve as a quasi-reference electrode.[26] Its potential was measured as −0.05 V vs. an Ag/Ag^+ reference electrode in our work, and thus the calculated potential of the AC electrode was 2.45 V (vs. Mg^{2+}/Mg), consistent with our previous reports.[5,27] The mass loading of AC was about 65 times that of NVP/C, and thus the voltage of the AC electrode would vary by less than 6 mV, considering the theoretical specific capacity of NVP (118 mA h g^{-1}) and the specific capacitance of AC (29 mA h g^{-1} V^{-1}). Therefore, a two-electrode coin cell system with $Mg(TFSI)_2$/MeCN as the electrolyte and an AC electrode as the counter electrode was used to test the electrochemical performance of NVP/C. Ti foil was used as the current collector and a linear-sweep voltage (LSV) test (Figure S3) revealed the Ti to be stable when it was charged to 3.05 V (vs. Mg^{2+}/Mg). To create vacant sites for Mg^{2+} ion insertion, two Na^+ ions in $Na_3V_2(PO_4)_3$ first had to be removed, and the resultant phase $NaV_2(PO_4)_3$ was used as the Mg^{2+} ion intercalation host. An electrochemical desodiation curve (Figure S4) showed a flat platform of around 2.5 V (vs. Mg^{2+}/Mg) and indicated a charge capacity of 98 mA h g^{-1}, corresponding to the extraction of 1.88 Na^+. ICP-AES analysis (Table 1) showed the atom molar ratio of Na to V in the original NVP electrode to be 1.503. After the desodiation process, the ratio decreased to 0.55 and the composition of the desodiated product was $Mg_{0.06}Na_{1.10}V_2(PO_4)_3$. The small amount of Mg^{2+} ions in the desodiated electrode came from the residual electrolyte, as determined from a control electrode that was soaked in the electrolyte without cycling. The desodiation process may be written as shown in Equation (1):

$$Na_3V_2(PO_4)_3 - 1.88\ Na^+ - 1.88\ e^- \rightarrow Na_{1.12}V_2(PO_4)_3 \quad (1)$$

To examine the electrochemical performance of ED-NVP/C as an Mg^{2+} ion intercalation host, galvanostatic charge–discharge tests were executed in the potential range 2.05–3.05 V (vs. Mg^{2+}/Mg). Figure 3a displays the charge–discharge voltage profiles of the first three cycles. The ED-NVP/C delivered a discharge capacity of 88.8 mA h g^{-1} with a coulombic efficiency of 107.8% in the first cycle. The chemical compositions of the magnesiated and demagnesiated electrodes (Table 1) were

Table 1. Chemical compositions of NVP electrodes during the electrochemical process. The theoretical compositions were calculated based on the electrochemical specific capacity. The experimental compositions were measured by ICP-AES.

NVP electrodes	Theoretical compositions	Experimental compositions
Original	$Na_3V_2(PO_4)_3$	$Na_{3.06}V_2(PO_4)_3$
Desodiated	$Na_{1.12}V_2(PO_4)_3$	$Mg_{0.06}Na_{1.10}V_2(PO_4)_3$
Magnesiated	$Mg_{0.85}Na_{1.12}V_2(PO_4)_3$	$Mg_{0.79}Na_{1.02}V_2(PO_4)_3$
Demagnesiated	$Na_{1.06}V_2(PO_4)_3$	$Mg_{0.04}Na_{1.08}V_2(PO_4)_3$

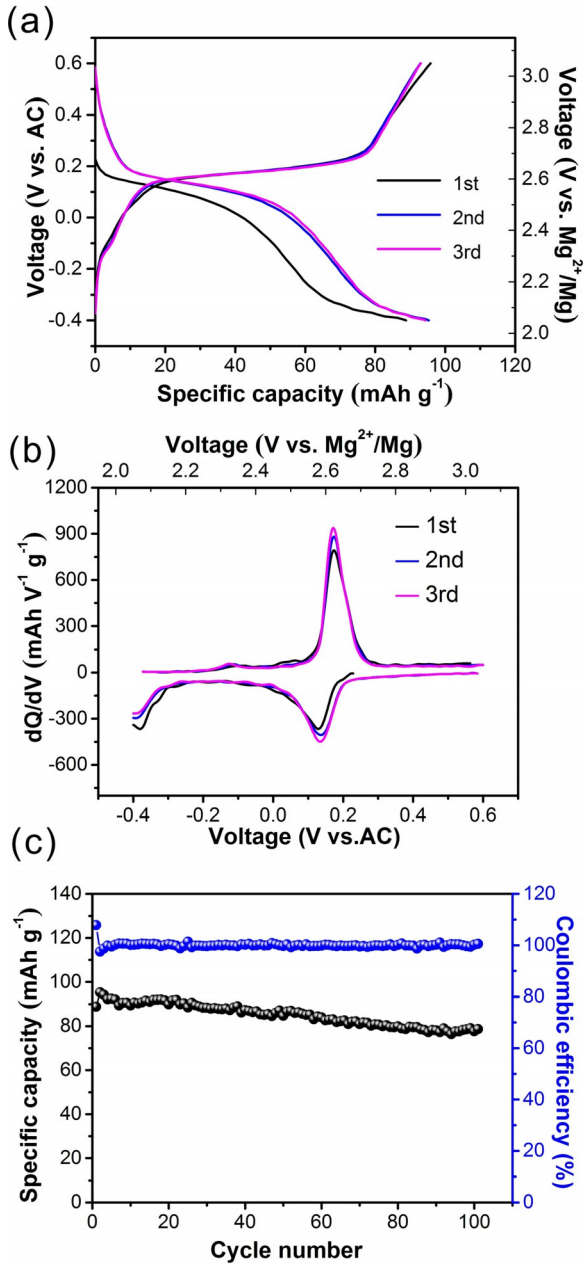

Figure 3. (a) Galvanostatic charge–discharge voltage profiles and (b) dQ/dV curves of the ED-NVP/C (the first three cycles at 20 mA g^{-1}); (c) cycle performance of the ED-NVP/C at 20 mA g^{-1}.

$Mg_{0.79}Na_{1.02}V_2(PO_4)_3$ and $Mg_{0.04}Na_{1.08}V_2(PO_4)_3$, respectively, consistent with the electrochemical results. In the second cycle, a higher discharge capacity of 95.3 mA h g^{-1} was obtained. This was probably due to the extraction of a small amount of remaining Na2 from the ED-NVP/C electrode, creating more vacant sites for Mg^{2+} ions to intercalate in the following cycle.[28] Differential capacity (dQ/dV) curves of the first three cycles derived from the obtained galvanostatic profile (Figure 3b) offer a better understanding of the charge–discharge process. As shown, the dQ/dV curve of the initial discharge process features a sharp peak at about 2.58 V (vs. Mg^{2+}/Mg) and a small peak at 2.07 V (vs. Mg^{2+}/Mg). The discharge dQ/dV curves of the 2nd and 3rd cycles are similar to that of the initial discharge curve, except that the peak intensity at 2.07 V decreases with increasing cycle number. For the charge process over the three cycles, a sharp peak at 2.62 V (vs. Mg^{2+}/Mg) as well as two weak peaks at 2.44 and 2.25 V (vs. Mg^{2+}/Mg) can be seen, indicating that the Mg^{2+} extraction process mostly occurs at 2.62 V (vs. Mg^{2+}/Mg). ED-NVP/C also showed good cycle performance (Figure 3c). At the 50th cycle, it still delivered 84.7 mA h g^{-1}, corresponding to a capacity retention ratio of 89.3% (based on the discharge capacity at the 2nd cycle). Even at the 100th cycle, 81% of the original capacity was maintained. The electrochemical performance of NVP/C was thus much better than that of the pristine NVP. It is noteworthy that the average working voltage of the ED-NVP/C was around 2.5 V (vs. Mg^{2+}/Mg), in good agreement with the expected value (2.6 V vs. Mg^{2+}/Mg) and much higher than those for most of the hitherto reported feasible cathode materials (Table S1 in the Supporting Information). This advantage provides a good opportunity to enhance the energy density of RMBs, since energy density can be effectively improved by increasing the voltage of the cathode.

Electrochemical reaction mechanism

Ex situ XRD analysis was conducted to investigate the structural evolution of the NVP/C during the processes of desodiation and (de)magnesiation in the 2θ range from 10° to 40° (Figure 4, Figure S5). Before the desodiation process, all of the peaks could be indexed to $Na_3V_2(PO_4)_3$, except for those at 35.02° and 38.43° originating from the Ti substrate. The calculated lattice constants of $Na_3V_2(PO_4)_3$ using the hexagonal axis were $a = 8.720(5)$ Å, $c = 21.760(5)$ Å, and volume = 1433.1(2) Å^3. During the Na^+ extraction process, the intensities of the peaks due to $Na_3V_2(PO_4)_3$ decreased and new peaks corresponding to $NaV_2(PO_4)_3$ developed. After the desodiation process, the remaining peaks for the ED-NVP electrode were consistent with an $NaV_2(PO_4)_3$ phase ($a = 8.417(5)$ Å, $c = 21.535(6)$ Å, and volume = 1321.4(5) Å^3), indicating a two-phase reaction between $Na_3V_2(PO_4)_3$ and $NaV_2(PO_4)_3$ during the desodiation process.[22] The decrease in the unit cell volume results from the shrinkage of the V–O bonds, whereas the P–O bond lengths remain unchanged, which contributes to the structural stability of NVP.[29] Upon discharging, reflections from the $NaV_2(PO_4)_3$ phase become weaker, while those from an intermediate phase corresponding to $Mg_xV_2(PO_4)_3$ (in this case, $x < 0.85$) are

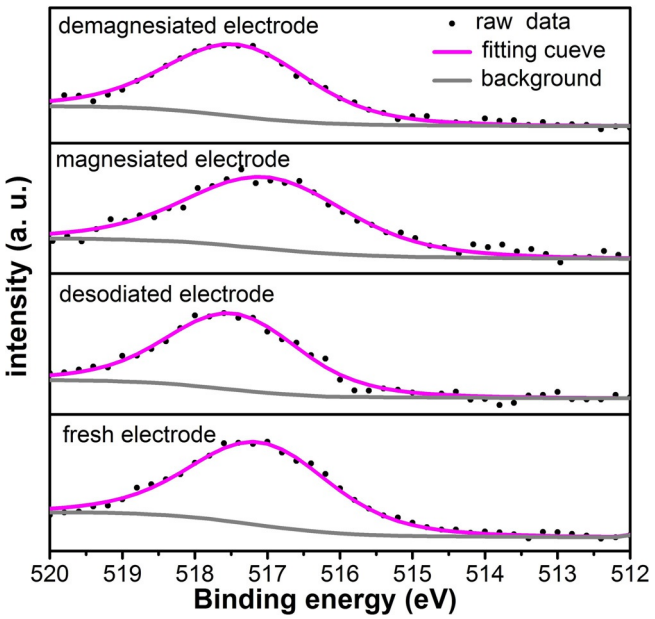

Figure 4. Ex situ XRD analysis of the NVP/C electrode during the desodiation process and the following (de)magnesiation process.

enhanced with increasing amount of inserted Mg^{2+} ions. Although some intermediate phases still remained at the end of the discharge process, the final reflections could still be traced to the NASICON parent.[13] The calculated lattice constants of the magnesiated phase were $a = 8.706(5)$ Å, $c = 21.720(2)$ Å, and volume = 1425.8(9) Å^3, indicating that both the a and c axes of the $NaV_2(PO_4)_3$ phase were enlarged by the intercalation of Mg^{2+} ions. Compared to the original $Na_3V_2(PO_4)_3$, the unit cell of the magnesiated phase was smaller, which might be attributed to the smaller size (Mg^{2+} 0.72 pm, Na^+ 1.02 pm) and strong polarity of Mg^{2+}. The recharging process corresponds to the demagnesiation process, and the extraction of Mg^{2+} ions leads to regeneration of the $NaV_2(PO_4)_3$ phase ($a = 8.416(9)$ Å, $c = 21.502(4)$ Å, and volume = 1319.2(2) Å^3). It has been reported that only two Na2 (18e sites) in $Na_3V_2(PO_4)_3$ can be extracted, and that the remaining Na1 will occupy the 6b sites in $NaV_2(PO_4)_3$.[11] Due to the smaller size of Mg^{2+} ions compared to Na^+ ions, it is expected that the former can insert into the available 18e sites in the $NaV_2(PO_4)_3$ phase with more readily.[16] Ex situ XRD results revealed that the (de)magnesiation process takes place through an intercalation–deintercalation mechanism with good reversibility.

XPS analysis was carried out to characterize the valence changes of vanadium during the electrochemical process. The desodiation process of the NVP/C and the subsequent (de)magnesiation process of the ED-NVP/C were expected to be accompanied by a redox process of $V^{4+} \leftrightarrow V^{3+}$. As shown in Figure 5, the $V2p_{3/2}$ peak of the fresh electrode located at 517.1 eV corresponds to V^{3+}.[12,30] The binding energy increased to 517.6 eV after the desodiation process, suggesting the oxidation of V^{3+} to V^{4+}.[31] During the subsequent magnesiation process, the $V2p_{3/2}$ peak shifted to lower binding energy (517.1 eV) and shifted back (517.7 eV) after the demag-

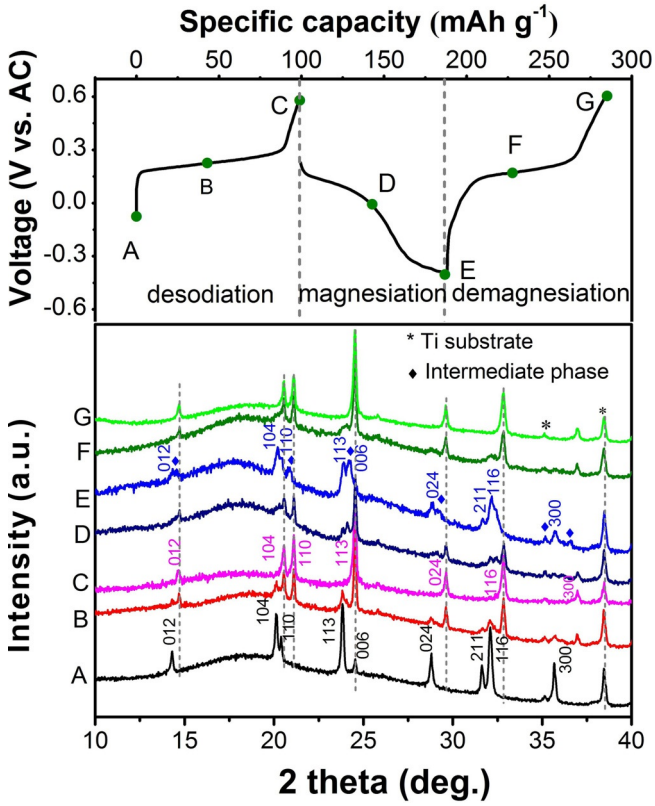

Figure 5. XPS spectra of $V2p_{3/2}$ of the NVP/C electrode during the desodiation process and the following (de)magnesiation process.

nesiation process. The XPS analysis thus provided further proof that the (de)magnesiation proceeded with good reversibility. According to the above analysis, the reaction mechanism based on electrochemical capacity during the magnesiation process can be written as shown in Equation (2):

$$Na_{1.12}V_2(PO_4)_3 + 0.85\ Mg^{2+} + 1.7e^- \rightarrow Mg_{0.85}Na_{1.12}V_2(PO_4)_3 \quad (2)$$

Mg^{2+} ion diffusion kinetics

The magnesium insertion/extraction kinetics into/from the ED-NVP/C was investigated by means of GITT. Figure 6a displays the GITT curves obtained during both the discharge and charge processes, which show a discharge plateau at 2.58 V (vs. Mg^{2+}/Mg) and a charge plateau at 2.62 V (vs. Mg^{2+}/Mg). The apparent diffusion coefficient for magnesium was calculated from the GITT curves. According to Fick's second law of diffusion, D_{Mg2+} can be calculated from Equation (3):

$$D_{Mg^{2+}} = \frac{4}{\pi}\left(\frac{m_B V_M}{M_B A}\right)^2 \left(\frac{\Delta E_s}{\tau\left(dE_\tau/d\sqrt{\tau}\right)}\right)^2 \left(\tau \ll L^2/D_{Mg^{2+}}\right) \quad (3)$$

where $D_{Mg^{2+}}$ ($cm^2\,s^{-1}$) is the magnesium diffusion coefficient, M_B and m_B are the molecular weight ($g\,mol^{-1}$) and the mass loading of active material (g), respectively, V_m is the molar volume of $Na_3V_2(PO_4)_3$ (141.98 $cm^3\,mol^{-1}$), A is the contact area between electrolyte and sample (here, for simplicity, the geometrical area of the electrode (1.1 cm^2) was used), τ (s) is the duration of the current pulse, and L is the thickness of the electrode (cm). If the relationship between E and $\tau^{1/2}$ is linear, Equation (3) can be further simplified to Equation (4):

$$D_{Mg^{2+}} = \frac{4}{\pi\tau}\left(\frac{m_B V_M}{M_B A}\right)^2 \left(\frac{\Delta E_s}{\Delta E_\tau}\right)^2 \quad (4)$$

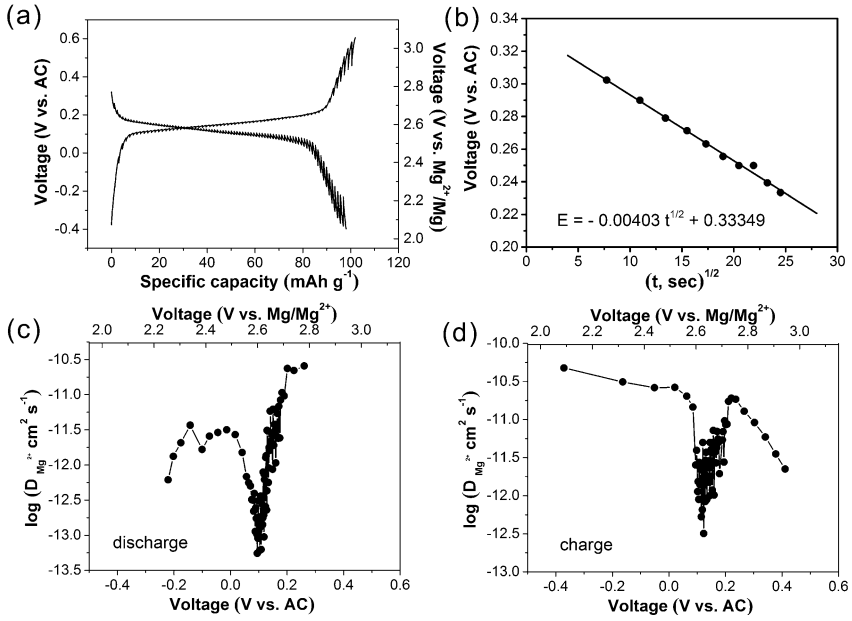

Figure 6. (a) GITT curve of the ED-NVP/C at 10 mA g^{-1}; (b) transient voltage of the galvanostatic pulse as a function of the square root of time for the ED-NVP/C; the apparent diffusion coefficients for magnesium calculated from the GITT curves for the ED-NVP/C electrode as a function of cell voltage during both the discharge (c) and charge (d) processes.

where ΔE_τ is the potential change during the current pulse without IR drop, and ΔE_s is the potential difference between the equilibrium states before and after the current pulse.

A linear relationship between E and $\tau^{1/2}$ (Figure 6b) validated the application of Equation (4) in the calculation of apparent diffusion coefficient for magnesium in this study. Figure 6c,d show the apparent diffusion coefficients for magnesium in both the discharge and charge processes. During the discharge process, the apparent diffusion coefficients were as high as 4.77×10^{-11} cm^2s^{-1} before and 9.62×10^{-12} cm^2s^{-1} after the plateau. For the charge process, values of 2.56×10^{-11} cm^2s^{-1} and 2.70×10^{-12} cm^2s^{-1} were determined before and after the plateau. Minimum apparent diffusion coefficients were obtained at the plateau for both the discharge (5.79×10^{-14} cm^2s^{-1}) and charge (5.31×10^{-13} cm^2s^{-1}) processes. A similar phenomenon has been observed in other phosphate-based materials, such as $LiFePO_4$ and $Li_3V_2(PO_4)_3$ in LIBs, and NVP in SIBs. This phenomenon indicates a two-phase transition and results from the strong interactions between the intercalated species and host material.[32] Thus, a similar explanation may also apply in this case, that is, the intercalation of Mg^{2+} ions into the ED-NVP/C by a two-phase transition.

Conclusion

In summary, mesoporous NVP/C spheres have been fabricated using a facile spray-drying–annealing method. After electrochemically extracting two Na^+ from the NVP/C, the desodiated electrode ED-NVP/C was evaluated as an insertion host for Mg^{2+} ions. Ex situ XRD and XPS analysis demonstrated that insertion of Mg^{2+} ions into ED-NVP/C is based on an intercalation–deintercalation reaction with good reversibility. GITT results revealed that the intercalation process takes place through a two-phase transition. The relatively high average working potential (ca. 2.5 V vs. Mg^{2+}/Mg) as well as good cycling stability make ED-NVP/C a promising high-voltage candidate material for use in RMBs. Our work also opens a way for exploring other NASICON-structured materials, such as $Na_3V_2(PO_4)_2F$, $Na_{1.5}VPO_4F_{0.5}$, and $Na_2FeTi(PO_4)_3$, as new kinds of high-voltage cathode materials for RMBs.[33]

Experimental Section

Materials: CH_3COONa, $NH_4H_2PO_4$, NH_4VO_3, and sucrose were analytical grade reagents and were purchased from Sinopharm Chemical Reagent Co., Ltd. Anhydrous acetonitrile (99.8%) was purchased from Shanghai Aladdin Bio-Chem Technology Co., Ltd. $Mg(TFSI)_2$ was purchased from Alfa Aesar. *N*-Methylpyrrolidene (NMP, battery grade), polyvinylidene fluoride (PVDF, battery grade), and acetylene black (battery grade) were purchased from Guangzhou Songbai Chemical Industrial Co., Ltd.

Synthesis: Typically, CH_3COONa (0.82 g, 0.01 mol), $NH_4H_2PO_4$ (1.15 g, 0.01 mol), and NH_4VO_3 (0.78 g, 0.0067 mol) were added to deionized water (100 mL). The mixture was stirred at 70 °C in a water bath for 1 h to obtain a transparent yellow solution. Sucrose (0.8 g) was then added as a carbon source, and the mixture was stirred for 0.5 h. The final solution was dried by means of a Büchi B-290 mini spray drier in an N_2 atmosphere, with an inlet temperature of 205 °C and an outlet temperature of 113 °C. The precursor was collected and annealed at 350 °C for 4 h and then at 750 °C for 8 h, attained at a heating rate of 5 °C min^{-1}, under 10% H_2/Ar atmosphere to obtain NVP/C. To obtain pristine NVP, the preparation process was the same, except for the omission of sucrose.

Characterization of the material: X-ray diffraction (XRD) patterns were measured on a Rigaku miniflex 600 diffractometer equipped with $Cu_{K\alpha}$ radiation. Scanning electron microscopy (SEM) images were collected with a Hitachi S-4800 instrument. Transmission electron microscopy (TEM) images were obtained with high-resolution transmission electron microscopes (HRTEM, JEM-2100 and FEI TECNAI G2 F30). Raman spectra were acquired with a Raman spectrometer (HORIBA Xplora). Nitrogen adsorption and desorption isotherms were investigated using the Brunauer–Emmett–Teller method (BET, Micromeritics surface area and porosity analyzer, ASAP 2020). Thermogravimetric (TG) measurements were conducted on an SDT-Q600 thermogravimetric analyzer at a heating rate of 10 °C min^{-1} from room temperature to 700 °C in air atmosphere. Inductively coupled plasma–atomic emission spectrometry (ICP-AES) analysis was conducted with a Plasma 1000 instrument. X-ray photoelectron spectroscopy (XPS) was performed on a Quantum 2000 scanning ESCA microprobe. For XPS and ex situ XRD analysis, electrodes were discharged or charged to certain states, then disassembled in a glovebox and washed with MeCN. The electrodes were sealed under Ar atmosphere with laminated aluminum film (used for LIBs) before being taken out of the glovebox and submitted to tests.

Electrochemical measurements: A slurry composed of 70 wt% as-prepared NVP/C, 20 wt% acetylene black, and 10 wt% PVDF was cast on a titanium (Ti) foil and dried at 80 °C in a vacuum oven overnight. Electrochemical performances were measured using CR2032 coin-type cells with Celgard 2400 as the separator and 0.3 M $Mg(TFSI)_2$/MeCN as the electrolyte. Activated carbon (AC) electrodes composed of 80 wt% AC (BET surface area >2000 m^2g^{-1}), 10 wt% acetylene black, and 10 wt% PVDF were used as both the counter and reference electrodes. The AC electrodes were dried at 100 °C in a vacuum oven at least for 48 h. The anodic stability of Ti in the electrolyte was measured by linear sweep voltammetry (LSV) from 0.2 to 1.5 V (vs. AC) at 5 mV s^{-1}. The electrochemical desodiation process of the NVP/C electrodes was performed in a two-electrode Swagelok's cell using AC electrodes as both the counter and reference electrodes and 0.3 M $Mg(TFSI)_2$/MeCN as the electrolyte. After charging to 0.6 V (vs. AC) at 20 mA g^{-1}, the Swagelok's cell was disassembled in a glove box and the desodiated electrodes (ED-NVP/C) were washed several times with MeCN to remove the residual Na^+ ions as far as possible. Galvanostatic charge–discharge tests of the ED-NVP/C electrodes were performed in the potential range -0.4 to $+0.6$ V (vs. AC) at 20 mA g^{-1} (0.17 C; 1 C = 118 mA g g^{-1}). For the galvanostatic intermittent titration technique (GITT) measurements, the cells were (dis)charged at a current density of 10 mA g^{-1} for 10 min, and this was followed by open-circuit relaxation for 1 h to reach the equilibrium state. The mass loadings of NVP/C were about 0.6 mg cm^{-2} for galvanostatic charge–discharge tests and 1.8 mg cm^{-2} for ex situ XRD measurements. All electrochemical measurements were carried out at room temperature.

Acknowledgements

We gratefully acknowledge the financial support of the National Natural Science Foundation of China (Grant Nos. 21273185 and 21321062) and the National Fund for Fostering Talents of

Basic Science (J1310024). The authors also thank Prof. D. W. Liao for his valuable suggestions.

Conflict of interest

The authors declare no conflict of interest.

Keywords: high-voltage cathode · intercalations · mesoporous materials · $Na_3V_2(PO_4)_3$ · rechargeable magnesium battery

[1] H. D. Yoo, I. Shterenberg, Y. Gofer, G. Gershinsky, N. Pour, D. Aurbach, *Energy Environmental Sci.* **2013**, *6*, 2265 – 2279.
[2] J. Muldoon, C. B. Bucur, A. G. Oliver, T. Sugimoto, M. Matsui, H. S. Kim, G. D. Allred, J. Zajicek, Y. Kotani, *Energy Environmental Sci.* **2012**, *5*, 5941 – 5950.
[3] I. Shterenberg, M. Salama, Y. Gofer, E. Levi, D. Aurbach, *MRS Bull.* **2014**, *39*, 453 – 460.
[4] D. Aurbach, Z. Lu, A. Schechter, Y. Gofer, H. Gizbar, R. Turgeman, Y. Cohen, M. Moshkovich, E. Levi, *Nature* **2000**, *407*, 724 – 727.
[5] G. Gershinsky, H. D. Yoo, Y. Gofer, D. Aurbach, *Langmuir* **2013**, *29*, 10964 – 10972.
[6] J. S. Kim, W. S. Chang, R. H. Kim, D. Y. Kim, D. W. Han, K. H. Lee, S. S. Lee, S. G. Doo, *J. Power Sources* **2015**, *273*, 210 – 215.
[7] Y. P. Zheng, Y. N. NuLi, Q. Chen, Y. Wang, J. Yang, J. L. Wang, *Electrochim. Acta* **2012**, *66*, 75 – 81.
[8] Y. Liu, L. Jiao, Q. Wu, Y. Zhao, K. Cao, H. Liu, Y. Wang, H. Yuan, *Nanoscale* **2013**, *5*, 9562 – 9567.
[9] a) S. Okamoto, T. Ichitsubo, T. Kawaguchi, Y. Kumagai, F. Oba, S. Yagi, K. Shimokawa, N. Goto, T. Doi, E. Matsubara, *Adv. Sci. (Weinheim)* **2015**, *2*, 1500072; b) Z. D. Huang, T. Masese, Y. Orikasa, T. Mori, K. Yamamoto, *RSC Adv.* **2015**, *5*, 8598 – 8603; c) Y. Orikasa, T. Masese, Y. Koyama, T. Mori, M. Hattori, K. Yamamoto, T. Okado, Z. D. Huang, T. Minato, C. Tassel, J. Kim, Y. Kobayashi, T. Abe, H. Kageyama, Y. Uchimoto, *Sci. Rep.* **2014**, *4*, 5622.
[10] Z. L. Jian, L. Zhao, H. L. Pan, Y. S. Hu, H. Li, W. Chen, L. Q. Chen, *Electrochem. Commun.* **2012**, *14*, 86 – 89.
[11] Z. Jian, C. Yuan, W. Han, X. Lu, L. Gu, X. Xi, Y.-S. Hu, H. Li, W. Chen, D. Chen, Y. Ikuhara, L. Chen, *Adv. Funct. Mater.* **2014**, *24*, 4265 – 4272.
[12] Q. Y. An, F. Y. Xiong, Q. L. Wei, J. Z. Sheng, L. He, D. L. Ma, Y. Yao, L. Q. Mai, *Adv. Energy Mater.* **2015**, *5*, 1401963.
[13] G. L. Li, Z. Yang, Y. Jiang, C. H. Jin, W. Huang, X. L. Ding, Y. H. Huang, *Nano Energy* **2016**, *25*, 211 – 217.
[14] Y. F. Li, Q. Y. An, Y. W. Cheng, Y. L. Liang, Y. Ren, C. J. Sun, H. Dong, Z. J. Tang, G. S. Li, Y. Yao, *Nano Energy* **2017**, *34*, 188 – 194.
[15] L. F. Wan, B. R. Perdue, C. A. Apblett, D. Prendergast, *Chem. Mater.* **2015**, *27*, 5932 – 5940.
[16] M. Cabello, R. Alcántara, F. Nacimiento, P. Lavela, M. J. Aragón, J. L. Tirado, *Electrochim. Acta* **2017**, *246*, 908 – 913.
[17] a) Y. Xu, Q. Wei, C. Xu, Q. Li, Q. An, P. Zhang, J. Sheng, L. Zhou, L. Mai, *Adv. Energy Mater.* **2016**, *6*, 1600389; b) X. Rui, W. Sun, C. Wu, Y. Yu, Q. Yan, *Adv. Mater.* **2015**, *27*, 6670 – 6676.
[18] W. Ren, Z. Zheng, C. Xu, C. Niu, Q. Wei, Q. An, K. Zhao, M. Yan, M. Qin, L. Mai, *Nano Energy* **2016**, *25*, 145 – 153.
[19] C. Zhu, K. Song, P. A. van Aken, J. Maier, Y. Yu, *Nano Lett.* **2014**, *14*, 2175 – 2180.
[20] a) A. B. D. Nandiyanto, K. Okuyama, *Adv. Powder Technol.* **2011**, *22*, 1 – 19; b) D. S. Jung, T. H. Hwang, S. B. Park, J. W. Choi, *Nano Lett.* **2013**, *13*, 2092 – 2097; c) X. P. Zhang, H. J. Guo, X. H. Li, Z. X. Wang, L. Wu, *Electrochim. Acta* **2012**, *64*, 65 – 70.
[21] a) J. Zeng, Y. Yang, C. Li, J. Li, J. Huang, J. Wang, J. Zhao, *Electrochim. Acta* **2017**, *247*, 265 – 270; b) Y. Yang, J. Li, J. Huang, J. Huang, J. Zeng, J. Zhao, *Electrochim. Acta* **2017**, *247*, 771 – 778; c) Y. Yang, J. Q. Li, X. Y. He, J. Wang, D. Sun, J. B. Zhao, *J. Mater. Chem. A* **2016**, *4*, 7165 – 7168; d) Y. Yang, J. Li, D. Chen, J. Zhao, *J. Electrochem. Soc.* **2017**, *164*, A6001 – A6006.
[22] Z. Jian, W. Han, X. Lu, H. Yang, Y.-S. Hu, J. Zhou, Z. Zhou, J. Li, W. Chen, D. Chen, L. Chen, *Adv. Energy Mater.* **2013**, *3*, 156 – 160.
[23] D. Zhao, M. Cao, *ACS Appl. Mater. Interfaces* **2015**, *7*, 25084 – 25093.
[24] E. Levi, Y. Gofer, D. Aurbach, *Chem. Mater.* **2010**, *22*, 860 – 868.
[25] W. Song, X. Ji, C. Pan, Y. Zhu, Q. Chen, C. E. Banks, *Phys. Chem. Chem. Phys.* **2013**, *15*, 14357 – 14363.
[26] P. W. Ruch, D. Cericola, M. Hahn, R. Kotz, A. Wokaun, *J. Electroanal. Chem.* **2009**, *636*, 128 – 131.
[27] Q. Y. An, Y. F. Li, H. D. Yoo, S. Chen, Q. Ru, L. Q. Mai, Y. Yao, *Nano Energy* **2015**, *18*, 265 – 272.
[28] D. M. Kim, Y. Kim, D. Arumugam, S. W. Woo, Y. N. Jo, M. S. Park, Y. J. Kim, N. S. Choi, K. T. Lee, *ACS Appl. Mater. Interfaces* **2016**, *8*, 8554 – 8560.
[29] K. M. Bui, V. A. Dinh, S. Okada, T. Ohno, *Phys. Chem. Chem. Phys.* **2015**, *17*, 30433 – 30439.
[30] J. C. Zheng, X. H. Li, Z. X. Wang, H. J. Guo, Q. Y. Hu, W. J. Peng, *J. Power Sources* **2009**, *189*, 476 – 479.
[31] G. Koyano, T. Okuhara, M. Misono, *Catal. Lett.* **1995**, *32*, 205 – 213.
[32] a) P. P. Prosini, M. Lisi, D. Zane, M. Pasquali, *Solid State Ionics* **2002**, *148*, 45 – 51; b) X. H. Rui, N. Ding, J. Liu, C. Li, C. H. Chen, *Electrochim. Acta* **2010**, *55*, 2384 – 2390; c) N. Böckenfeld, A. Balducci, *J. Solid State Electrochem.* **2014**, *18*, 959 – 964.
[33] S. Chen, C. Wu, L. Shen, C. Zhu, Y. Huang, K. Xi, J. Maier, Y. Yu, *Adv. Mater.* **2017**, 1700431.

Manuscript received: September 13, 2017
Accepted manuscript online: September 27, 2017
Version of record online: November 7, 2017